Available online at www.sciencedirect.com
SCIENCE DIRECT®
Journal of Magnetic Resonance 173 (2005) 40–48
JMR Journal of Magnetic Resonance
www.elsevier.com/locate/jmr

Communication

Reduction of RF-induced sample heating with a scroll coil resonator structure for solid-state NMR probes

John A. Stringer[a], Charles E. Bronnimann[a], Charles G. Mullen[a], Donghua H. Zhou[b], Sara A. Stellfox[b], Ying Li[b], Evan H. Williams[c], Chad M. Rienstra[b,*]

[a] *Varian, Inc., 2607 Midpoint Drive, Fort Collins, CO 80525, USA*
[b] *Department of Chemistry, University of Illinois, 600 South Mathews Avenue, Urbana, IL 61801, USA*
[c] *Varian, Inc., 3120 Hansen Way, Palo Alto, CA 94304-1030, USA*

Received 17 September 2004; revised 4 November 2004
Available online 15 December 2004

Abstract

Heating due to high power ^{1}H decoupling limits the experimental lifetime of protein samples for solid-state NMR (SSNMR). Sample deterioration can be minimized by lowering the experimental salt concentration, temperature or decoupling fields; however, these approaches may compromise biological relevance and/or spectroscopic resolution and sensitivity. The desire to apply sophisticated multiple pulse experiments to proteins therefore motivates the development of probes that utilize the RF power more efficiently to generate a high ratio of magnetic to electric field in the sample. Here a novel scroll coil resonator structure is presented and compared to a traditional solenoid. The scroll coil is demonstrated to be more tolerant of high sample salt concentrations and cause less RF-induced sample heating. With it, the viable experimental lifetime of a microcrystalline ubiquitin sample has been extended by more than an order of magnitude. The higher B_1 homogeneity and permissible decoupling fields enhance polarization transfer efficiency in ^{15}N–^{13}C correlation experiments employed for protein chemical shift assignments and structure determination.

Keywords: Solid-state NMR spectroscopy; Solenoid; Scroll; Probe; Heating; Salt; Dielectric; Protein

1. Introduction

In recent years, applications of multi-dimensional solid-state NMR (SSNMR) to uniformly labeled peptides and proteins have increased dramatically in number and scope [1,2]. One essential ingredient for the success of these experiments is a microscopically well-ordered sample with minimal inhomogeneous contributions to the ^{13}C and ^{15}N line widths. Although under favorable circumstances lyophilized, rehydrated protein samples may yield satisfactory resolution [3,4], several studies have demonstrated that optimal resolution for magic-angle spinning (MAS) experiments is likely to be observed in samples that are precipitated or crystallized in a manner mimicking single crystal growth [5–9]. Likewise, the preparation of oriented proteins in lipid bilayers requires that hydration be maintained to achieve optimal resolution [10]. These approaches to SSNMR sample preparation offer the advantage that single crystals are not required; an unfortunate technical consequence is that microcrystals or hydrated bilayers often have a significant salt concentration.

SSNMR probes have not historically been designed to perform optimally with high ionic strength protein samples. Dielectric loading and electrical conductivity of the mother liquor surrounding the protein (and/or the dielectric properties of the protein itself) can severely compromise probe performance and reduce sample lifetime. Tuning of the ^{1}H (and/or ^{19}F) channel may be

* Corresponding author. Fax: +1 217 244 3186.
E-mail address: rienstra@scs.uiuc.edu (C.M. Rienstra).

1090-7807/$ - see front matter © 2004 Elsevier Inc. All rights reserved.
doi:10.1016/j.jmr.2004.11.015

completely lost in many circuits with as little as 100 mM salt. If the probe can be tuned, pulse widths and sensitivity on the ^{1}H channel are compromised. These problems parallel similar issues observed in solution NMR, which are most evident in cryogenic probes due to their extremely high unloaded quality factor (Q); the use of buffers with lower ion mobility, as well as ionic strength, can improve performance in this context [11]. However, in SSNMR the application of high power ^{1}H decoupling exacerbates the problem: incident decoupling power of ~100 Watts (W) for tens to hundreds of milliseconds can result in temperature jumps of greater than ~50 °C (vide infra). Because the dielectric heating experienced by the sample is proportional to f^{3} (where f is the frequency of the irradiating field) [12], the effect of high-power ^{1}H decoupling is 64 times greater than a comparable duty cycle ^{13}C TOCSY experiment. Performing experiments under such conditions can cause rapid sample deterioration, and even in the short term can reduce resolution due to temperature gradients across the sample, in cases where chemical shifts are temperature-dependent.

Thus far, many investigators have avoided the most severe implications of these technical limitations by accepting compromises in SSNMR experimental performance. For example, although it is well known that the residual dipolar line widths continue to decrease with ^{1}H decoupling powers well beyond 100 kHz [13], most protein studies have utilized decoupling fields of ~70 kHz during the evolution and detection dimensions [7,9,14–16]. The primary exception was a study of BPTI in which the microcrystalline sample was prepared at essentially zero salt concentration, permitting ~140 kHz decoupling fields to be employed without immediate sample degradation [17]. Furthermore, polarization transfer in most 2D and 3D experiments on proteins so far has relied upon dipolar recoupling pulse sequences such as proton driven spin diffusion (PDSD) [18], DARR [19], RFDR [20], and SPECIFIC CP [21], due explicitly to limitations in the available decoupling power that could be utilized. Pulse sequences with windowless RF pulse trains—such as DRAWS [22], C7 [23], SPC-5 [24], and other symmetry-based sequences [25,26]—have been demonstrated to provide superior performance in model compounds and small peptides (e.g., prepared by evaporation of organic solvents with a low dielectric constant) [27], yet have so far been utilized infrequently for hydrated protein samples, because the combination of high power ^{13}C (and/or ^{15}N) pulses with proportionate increases in ^{1}H decoupling power causes rapid protein sample deterioration. At fast MAS rates these sequences, even without any ^{1}H decoupling [28], might be superior to simpler experiments. Likewise, low power ^{1}H decoupling [29] during chemical shift evolution periods appears to be viable as a way of reducing RF heating in the fast MAS limit; the low-power XiX sequence [30] makes optimal use of available RF power, but does not yet achieve the level of performance observed in the very high decoupling field limit.

The ^{1}H decoupler heating effect can be mitigated by preparing samples at low salt concentrations (<10 mM). Unfortunately many proteins fail to crystallize without sufficient concentrations of salt; thus, the majority of conditions in commercial hanging drop vapor diffusion kits have more than 100 mM salt. For example, the Crystal Screen Lite kit (Hampton Research, Aliso Viejo, CA) is optimized for low ionic strength, yet most of its conditions contain at least 200 mM salt and/or 100 mM buffer. Although it is sometimes possible to find microcrystal conditions at even lower salt concentrations, many protein–protein interactions occur specifically among charged surface residues; substantial reductions in ionic strength might fundamentally alter the structure of such proteins and/or their affinity for ligands. Therefore in many instances it is necessary or desirable to examine samples at high ionic strength.

One might also mitigate sample deterioration by performing NMR experiments far below room temperature (~100 K), a strategy commonly employed in X-ray diffraction studies using high intensity synchrotron beams (see, for example [31]). However, solid-state NMR studies near physiological temperatures may also be required, in order to resolve specific discrepancies between solution NMR and X-ray crystal structures [32] or to report on dynamic events as a function of temperature [33].

In this Communication, we present results from a scroll coil resonator design that addresses many of these issues. This resonator is especially well suited to multi-channel SSNMR probes, since it is compatible with electronic circuits originally designed for solenoid sample coils. We demonstrate that the loaded circuit Q, pulse widths and RF-induced heating effects of the scroll coil probe as a function of salt concentration are substantially improved relative to a solenoid with similar geometry. Thus, we expect that this strategy will extend sample lifetime and expand the range of sample conditions accessible to SSNMR. Furthermore, the improved B_1 homogeneity and permissible ^{1}H decoupling fields in this design increase polarization transfer efficiency and therefore sensitivity in 2D and 3D experiments.

2. Background

Dielectric loading of a sample resonator can be minimized by decreasing coil inductance, for example, by reducing the number of turns in the classic solenoid design. However, in most SSNMR multi-channel probe designs, the efficiency and overall sensitivity of the low frequency channels (^{31}P, ^{13}C, ^{15}N, etc.) is proportional

to the coil inductance (due both to the fundamental circuit analysis as well as parasitic inductance around the MAS module) [34,35]. Reducing the inductance by an order of magnitude in solenoid designs would therefore result in unacceptable sensitivity losses on ^{13}C and ^{15}N. Furthermore, B_1 homogeneity (in the low frequency limit) is degraded as the number of turns in a solenoid is decreased. The loop gap resonator (LGR) structure, originally developed for EPR spectroscopy [36,37], is well suited to high frequency, single channel designs, including low frequency EPR [38]. The LGR offers excellent B_1 homogeneity for NMR applications as well [39], and has been extended to a multiple resonance concept by inductive flux linkage within a solenoid, which is tuned to the low frequency channels [40]. One drawback of this approach is that the LGR has an inductance on the order of 2–3 nH (for a ~3.6 mm inner diameter compatible with 3.2 mm rotor geometry), requiring a relatively large parallel capacitance (~10–50 pF) to resonate between 500 and 900 MHz. This capacitance is typically generated by small case ceramic chip capacitors (e.g., American Technical Ceramics, Huntington Station, NY), which may compromise voltage-handling and thermal properties in the context of high-power ^{1}H decoupling experiments.

Aiming to exploit the high homogeneity and low electric (E) field of the LGR, but achieve acceptable power-handling and low frequency channel performance, we explored the scroll coil (or "Swiss roll") [41]. This resonant structure combines many of the favorable design features of both the LGR and the solenoid. The scroll coil behaves, to first order, like a LGR at the high frequency, but with a larger inductance and sufficient parallel capacitance between turns of the coil to resonate near the desired ^{1}H frequency (~500–900 MHz). The parallel capacitance has little effect at the lower frequencies; thus, the structure behaves very much like a solenoid at the ^{13}C and ^{15}N frequencies, and can therefore be incorporated into triple resonance SSNMR probe circuits [42]. We anticipated that this hybrid structure might improve salt tolerance and decrease RF heating, while retaining acceptable performance on the lower frequency channels of the probe.

3. Results and discussion

We first investigated whether the scroll coil had sufficient Q to be competitive in a SSNMR probe circuit. We constructed a scroll coil structure (3.6 mm inner diameter, 6.7 mm length, four turns) from 70 μm (2.8 mil) thick copper with 150 μm (6 mil) thick polytetrafluoroethylene (PTFE) dielectric between turns. Bench top measurements showed the unloaded Q of this scroll coil at 500 MHz to be 190, in comparison to an unloaded solenoid with similar geometrical parameters (~3.6 mm inner diameter, 6.4 mm length, eight turns), which had a Q of 200. Both coils were tuned to resonant tank circuit consisting of a $\sim\lambda/4$ ^{1}H resonator with variable electrical length (dielectric slug) tuning and Varian tuning tube technology (T3) for the ^{13}C and ^{15}N isolation and tuning circuits. This circuit is a modern version of the Cross–Hester–Waugh topology [34], which has been modified for high frequency by Zilm and co-workers [43].

The ^{1}H field strength as a function of incident power for the scroll coil ($\omega_1/2\pi = \gamma B_1/2\pi = 83$ kHz at 35 W incident power) was better than for a solenoid (83 kHz at 50 W). We attribute this observation to the improved filling factor of the scroll coil, which offers excellent B_1 homogeneity in comparison to the solenoid; the majority of the flux generated contributes to B_1 in the sample region. (The extremely low flux leakage of the scroll coil has also been utilized for imaging applications [44].) The 30% reduction in power required to achieve 83 kHz on the scroll probe (relative to the solenoid) represents the lower bound on the improvement in performance observed on the scroll probe at 500 MHz, because here we have determined B_1 fields by measurement of 2π and π pulse lengths (i.e., $\omega_1/2\pi = (1/2)/(\tau_{2\pi} - \tau_{\pi})$), which accurately reports on the peak field in the coil, but underestimates the average field. RF nutation profiles (presented below) are a more accurate indicator of the overall field homogeneity of the scroll coil, and along with experimental measurements of B_1 field as a function of position along the coil axis, indicate that the overall field per coil volume is 28% higher in the scroll coil than in the solenoid. Furthermore, for higher frequency applications, the scroll coil follows very closely to the expected trend for Q (proportional to $\sqrt{f}$) up to at least 900 MHz, whereas the solenoid peaks at ~300–400 MHz and begins to fall off rapidly above 500 MHz. (The same geometry scroll coil was utilized over the range from 500 to 900 MHz; the precise relationship of the ^{1}H frequency to the self-resonant frequency of the scroll coil has minimal impact on overall ^{1}H circuit performance.) Preliminary NMR tests of scroll probes at 750 and 800 MHz confirm this trend, and significantly greater improvements in ^{1}H sensitivity therefore may be possible at high frequencies.

Conversely, at low frequencies the performance of scroll probe falls short of the solenoid, if using the simplest metric of pulse widths as a function of incident power. For example, at the ^{13}C frequency (125 MHz), 89 kHz peak fields were achieved with 213 W on the solenoid coil probe, compared to 50 kHz with 220 W on the scroll probe; on the ^{15}N channel (50 MHz), the power required to generate a 50 kHz field increased from 300 W (solenoid) to 750 W (scroll). These factors arise from the lower coil inductance (22 nH) and probe Q for the scroll probe (total circuit $Q = 56$ at 50 MHz), versus the solenoid (83 nH and $Q = 71$).

Assuming the NMR detection sensitivity on ^{13}C and ^{15}N to be determined directly by reciprocity arguments [45], the measured pulse widths would predict approximately 37–45% reductions in sensitivity on these channels. In practice, sensitivity of the scroll probe on both ^{13}C and ^{15}N is closer to the solenoid than this simplified analysis would predict, due to the RF filling factor arguments discussed already and because the performance of pulse sequences for transferring polarization among ^{1}H, ^{13}C, and ^{15}N nuclei benefit disproportionately from the improved B_1 homogeneity of the scroll probe. These issues become especially important in the context of 3D experiments on proteins, as discussed further below.

We proceeded to evaluate performance with high dielectric samples. The Q of the scroll probe (^{1}H channel) is altered minimally, in comparison to changes in the solenoid by more than a factor of two (Fig. 1). Whereas the solenoid loaded Q decreased by almost 50% as the salt concentration increased from 0.1 to 0.94 M, the scroll Q decreased by less than 10%, with the ^{1}H pulse widths closely following the expected $(\sqrt{1/Q_L})$ dependence. Moreover, the shift in the resonant frequency of the probe reliably reported on the resonator sensitivity to salt. In practice, the standard tuning range of the ^{1}H channel of most SSNMR probes with solenoid sample coils is not sufficient to recover tuning in samples of >150 mM; we made especially large

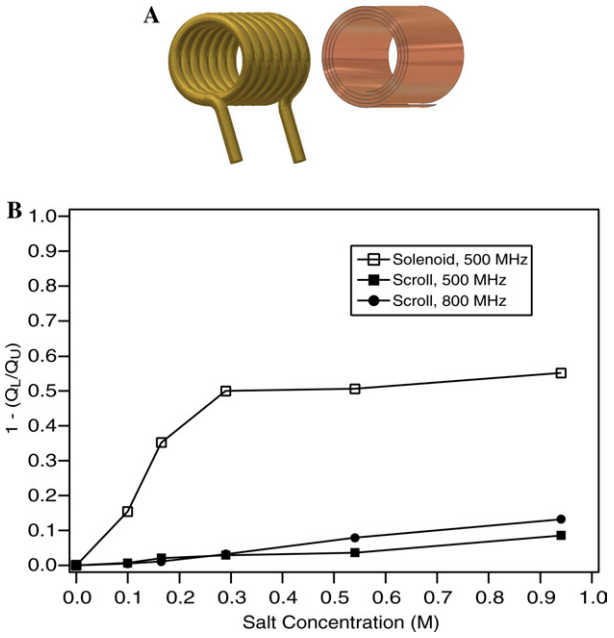

Fig. 1. (A) Schematic drawings of solenoid and scroll coil resonator with similar geometrical parameters. The scroll coil is fabricated from a conductive material wrapped around a cylindrical support, with dielectric spacing between turns. (B) Effect of dielectric loading on the quality factor of scroll and solenoid coils. The parameter $1-(Q_L/Q_U)$ (where Q_L is the loaded Q and Q_U the unloaded Q) is plotted as a function of salt concentration (aqueous NaCl). Data at 500 MHz are presented for both the scroll and solenoid, and at 800 MHz for the scroll only, as indicated in the legend.

corrections to the transmission line tuning circuit to recover tuning for the solenoid. The circuit equipped with the scroll coil shifted ^{1}H resonant frequency by only a fraction of a MHz over the entire range of ionic strength examined here. This reduction in sample loading results directly from the minimal conservative electric field of the scroll resonator, which can be visualized by considering the applied potential to each structure (solenoid and scroll) and the resulting E field. The solenoid driving potential is applied along the axis of the coil, so the generated E fields penetrate the sample volume. For the scroll, the driving potential is applied from the inner to outer turn, so little E field is generated within the sample region; this result optimizes the use of the applied potential and minimizes dependence upon sample dielectric properties. Therefore the overall ^{1}H channel performance on the scroll coil probe was improved by a substantial margin, and remains functional for high-power decoupling applications even at near 1 M ionic strength.

Next we compared steady-state heating effects, using the chemical shift thermometer thulium 1,4,7,10-tetraazacyclododecane-1,4,7,10-tetrakis(methylene phosphonate) ($TmDOTP^{5-}$) [46], in aqueous solution with varying amounts of salt (NaCl). Fig. 2A illustrates the average sample heating as a function of incident power, normalized to common nutation field squared. (This unit permits facile comparison of probes with different overall efficiency, since heating effect per unit B_1 field is the parameter of interest; the square of the field is used to produce a linear plot, where the slope corresponds to the probe-specific heating as a function of average decoupling power.) At the 940 mM salt concentration, the temperature rise of the solenoid probe was 1.00 ± 0.06 °C/kHz^2, compared to 0.069 ± 0.004 °C/kHz^2 for the scroll; at 160 mM, the heating from the solenoid was 0.45 ± 0.03 °C/kHz^2, and the scroll, 0.028 ± 0.002 °C/kHz^2. At lower ionic strength, the heating effect is approximately linear in the salt concentration. However, in all cases the heating is ~14–16 times greater per unit power (or field squared) for the solenoid than the scroll. Furthermore, the temperature gradient is significantly worse for the solenoid; as illustrated in Fig. 2B, for the 165 mM ionic strength sample at the average power of 38 kHz^2, there is an asymmetric ~12 °C gradient in addition to the ~20 °C mean temperature shift. For the scroll, the gradient with this power level is negligible; with almost ten times more average power (273 kHz^2), the gradient is only one fourth (~3 °C) of that observed with the solenoid, with an average temperature rise of 9 °C. Thus, the average heating per unit power is 16 times less than with the solenoid, and the gradient per unit power is approximately 30 times less.

Clearly the extent of heating with the solenoid is prohibitive for most proteins. Typical protein MAS experi-

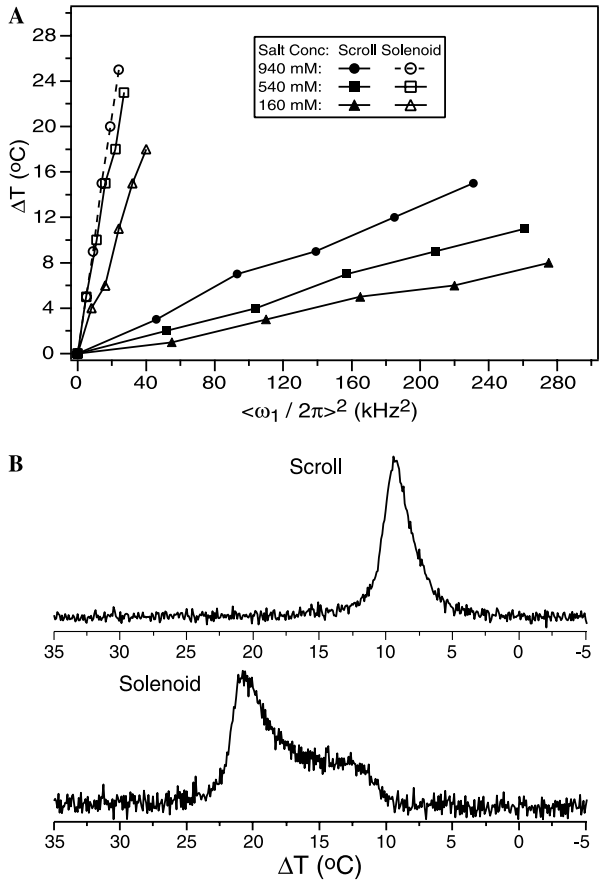

Fig. 2. Measurements of RF-induced sample heating at 500 MHz ^{1}H frequency. (A) Plot of average sample heating in solenoid and scroll coil probes with salt solutions of various ionic strength. A variable time presaturation pulse modulated the total duty cycle of RF irradiation; a delay after presaturation of ~15 ms was sufficiently long compared to the T_1 of the ^{1}H signals close to the paramagnetic site. The x-axis is presented as a nutation frequency squared to produce a line whose slope depends upon the probe-dependent heating. (B) 1D ^{1}H spectrum of the sample with 165 mM salt concentration at the highest average applied field (231 kHz^2 for the scroll, and 27 kHz^2 for the solenoid) with x-axis adjusted to reflect the relative temperature change (in °C) of the H6 resonance of DOTP (at ca. −155 ppm) ($C_T = 0.87$ ppm/°C [46]). The 0 °C reference point was determined in the limit of low applied RF power, by analyzing the convergence of all ^{1}H signals in DOTP as previously described in [46].

ments employ a maximum of 50 ms ^{1}H decoupling at ~70 kHz, with pulse delays of 2 s, resulting in a ~2.5% duty factor and average power of 122.5 kHz^2. These levels applied to the 160 mM sample would cause steady-state heating of 55 °C using a solenoid. An additional concern is that the power is delivered in short pulses (i.e., fast compared to the rate of thermal conduction throughout the sample) and the electric field is asymmetric over the sample geometry. Transient heating effects in the hottest portions of the sample are likely to exceed the unfolding transition temperatures for even the most robust proteins. We have found that deteriorated protein samples have regions of discoloration (from white to yellow, brown or black) whose position correlates well with the known region of maximum electrical field in the coil.

Next we performed a direct comparison of heating on ^{15}N labeled samples of microcrystalline human ubiquitin prepared by methylpentanediol precipitation according to a previously published protocol [9]. We employed aggressive decoupling conditions of 75 kHz for 120 ms with a 1.5 s recycle delay, for a 7.5% total duty factor (average power of 422 kHz^2). Fig. 3A shows 1D spectra acquired every hour for 16 h in the scroll probe. No significant changes were observed in the sample integrity. The same 1D experiments were then performed in the solenoid probe (Fig. 3B). Rapid degradation of this sample is evident despite the fact that the salt concentration is only 8 mM; the effective ionic strength in the solid portion of the sample is likely to be increased by the protein itself, since the protein concentration in the rotor is ~25 mM, and ubiquitin contains 11 residues (4 Arg and 7 Lys) that are certain to be positively charged at this pH and 10 others (4 Asp and 6 Glu) that could be negatively charged, depending on their effective pKa's in the crystal. Even within the first hour in the solenoid probe, the sample shows signs of deterioration, which proceed from minor broadening in the first few hours to a complete disappearance of the outlying (downfield) Pro and Ala ^{15}N resonances after 16 h. With the scroll probe, several other samples with salt concentrations as high as 40 mM were subjected to similar average (and significantly greater peak) RF power levels for periods of several hours to days each. In no case was significant RF-induced deterioration observed with the samples in the scroll coil probe. It appears that an order of magnitude higher duty factor would be required to do so.

We proceeded to perform a high-power triple resonance 3D ^{15}N–^{13}CO–^{13}CX experiment (Fig. 4), to confirm whether triple resonance irradiation could be tolerated with unusually high duty factors in the scroll probe. The experimental parameters (as described in the caption to Fig. 4) resulted in an average ^{1}H field^2 of 478 kHz^2. Despite the fact that only ~3 mg of protein was packed in this 3.2 mm rotor, this 3D spectrum was acquired in 11.0 h. The sample integrity was confirmed by analyzing peak positions consistent with the published SSNMR assignments of ubiquitin [9,16]. Sensitivity (signal-to-noise ratio) of the observed N–CO[$i-1$]–CO[$i-1$] peaks averaged 15:1, the N[i]–CO[$i-1$]–Cα[$i-1$] ~10:1, and the N[i]–CO[$i-1$]–Cβ[$i-1$] ~7:1. The overall limitation to sensitivity in this case was the ^{1}H–^{15}N CP step, where further gains are possible. A direct comparison of the sensitivity of this experiment under these circumstances was not possible due to sample deterioration observed in the solenoid probe.

One drawback of the scroll coil is that ^{13}C (and ^{15}N) sensitivity is reduced in 1D spectra of standard SSNMR model compounds at identical decoupling and cross

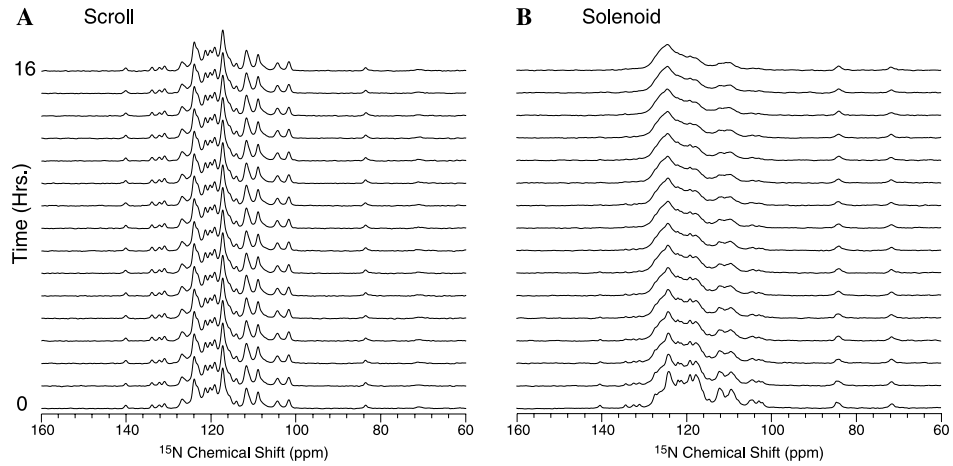

Fig. 3. Time-dependent 1D ^{15}N spectra of microcrystalline ubiquitin in the scroll and solenoid probes. The ^{15}N protein (~5 mg) was precipitated with methylpentanediol at pH 4.0 with a final salt (sodium citrate and citric acid) concentration of 8 mM, and packed into an air-tight 3.2 mm rotor (sealed with silicone rubber disks cut from 1.5 mm thick sheet (McMaster-Carr PN 8632K921) and cylindrical Kel-F spacers). The MAS rate was 13.333 kHz. 1D ^{15}N CP-MAS acquisition parameters were: 2 ms ^{1}H–^{15}N CP (at ~43 kHz ^{1}H, 30 kHz ^{15}N with a tangent ramp), 75 kHz decoupling for 120 ms, 1.5 s pulse delay. On the left are the stacked spectra from an overnight run (1 h per spectrum) on the scroll probe. On the right are results from the same experiment an otherwise equivalent design with solenoid coil.

polarization levels. However, in practice there are several reasons that sensitivity in 2D and 3D experiments with proteins will be enhanced by the scroll coil design. First, higher available decoupling levels during evolution and acquisition periods will narrow line widths and increase peak heights; these effects are often linear in the applied decoupling field. Second, protein experiments often are performed with recycle delays limited by the steady state sample heating. The signal-to-noise per unit time in a CP experiment (presuming all polarization comes from ^{1}H nuclei) is proportional to $(1-e^{-\tau/T_1})\sqrt{1/\tau}$, where τ is the time per scan (assumed large compared to the acquisition time), and T_1 is the longitudinal ^{1}H relaxation rate. This function is maximized when $\tau = \sim 1.25\,T_1$. Therefore for proteins, where ^{1}H T_1 values are typically 400–800 ms, reducing the experimental pulse delay from 2 to 1 s would increase sensitivity per unit time by 10% (^{1}H T_1 of 800 ms) to 30% (T_1 = 400 ms). Third, the overall sensitivity in heteronuclear 2D or 3D experiments depends strongly upon the polarization transfer efficiency between ^{15}N and ^{13}C nuclei. This efficiency can be improved by large factors, especially at high B_0 field, with the availability of higher decoupling fields and more homogeneous B_1 fields (Fig. 5A). For example, we explored the optimal regime of tangent ramp sizes and mixing times in double cross polarization experiments with *N*-acetyl-valine (NAV). We found that especially small ramp sizes were optimal, in comparison to experiments performed on the solenoid probe; smaller ramps may be especially beneficial when $T_{1\rho}$ relaxation is short, as for proteins in the intermediate exchange motional regime. For NAV, the smaller ramps resulted in a ~50% polarization transfer from ^{15}N to ^{13}Ca (normalized to the direct ^{1}H–^{13}C CP spectrum with similar optimizations of ramp size and shape), despite leakage of ~10% more signal to the ^{13}Cb. Furthermore, the decoupling dependence in this polarization transfer to a protonated ^{13}C was especially strong: the ^{13}Ca signal intensity more than doubles by increasing the decoupling field from 90 to 100 kHz, and doubles again upon increasing from 100 to 120 kHz (Fig. 5B). If the ^{1}H decoupling field were reduced by ~20% due to dielectric loading of a high ionic strength sample, a typical value in the solenoid probe with the ubiquitin samples described above, the sensitivity of the 2D or 3D experiment would therefore suffer by a factor of two or more.

Further investigations into pulse sequence performance in the regime of high B_1 homogeneity will be required to understand the ultimate limits of polarization transfer efficiency and resolution in protein samples. However, it is safe to conclude that high B_1 homogeneity will ultimately lead to additional improvements in polarization transfer efficiency and resolution, and relaxing the technical limitation on ^{1}H decoupling levels in protein experiments will likewise be beneficial in many experiments.

4. Conclusions

We have presented a new resonator design for SSNMR probes, which offers greatly improved tolerance to salt and reduced dielectric heating, as well as excellent B_1 homogeneity. The primary application of this design is for samples whose ionic strength is too high for traditional solenoid designs. However, we expect that even for samples with relatively low (~10–100 mM) salt concentrations, significant benefits will be realized from the lower electric fields experienced by the sample. In our

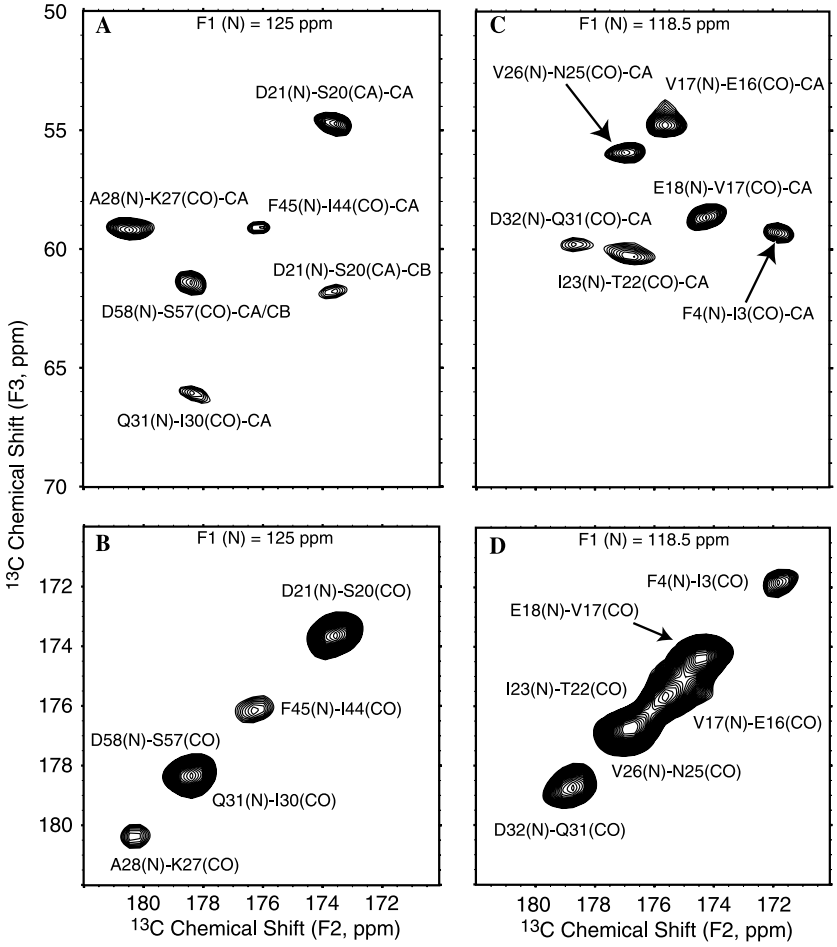

Fig. 4. 3D ^{15}N–^{13}CO–^{13}CX experiment performed with the 600 MHz scroll coil probe on a microcrystalline ^{13}C,^{15}N ubiquitin sample (~3 mg), prepared in the same manner as described in Fig. 3. 2D ^{13}CO–^{13}CX planes at various ^{15}N frequencies: (A) ^{13}CO–^{13}Cα and (B) ^{13}CO–^{13}CO regions at F1 (^{15}N) = 125 ppm. (C) ^{13}CO–^{13}Cα and (D) ^{13}CO–^{13}CO regions at F1 (^{15}N) = 118.5 ppm. The visible depth in the F1 dimension is ±0.8 ppm. Assignments were made in accordance with [9,16]. Experimental parameters: 2.4 μs ^{1}H π/2 pulse; 3 ms ^{1}H–^{15}N CP at $\omega(^{1}H)/2\pi = 32$ kHz, $\omega(^{15}N)/2\pi = 18$ kHz with a ±5 kHz tangent ramp [51]; 96 × 75 μs (TPPI) [52] in t_1 (^{15}N); 10 ms ^{15}N–^{13}CO CP at $\omega(^{15}N)/2\pi = \sim 18$ kHz, $\omega(^{13}C)/2\pi = \sim 31$ kHz (at 172 ppm) [21] with a ±2 kHz tangent ramp and CW $\omega(^{1}H)/2\pi = 105$ kHz decoupling; 96 × 75 μs (TPPI) in t_2 (^{13}CO); 25 ms DARR [19] ^{13}C–^{13}C mixing with $\omega(^{1}H)/2\pi = 13.3$ kHz; 5 μs ^{13}C π/2 pulses; 2048 × 15 μs (complex) in t_3 (^{13}C); ~95 kHz TPPM [53] with $t = 5.1$ μs and $\phi = 15°$ during the evolution and acquisition periods; 82 ms total irradiation time; four scans per row; 1 s pulse delay; 7.5% duty factor; $\langle\omega(^{1}H)/2\pi\rangle^2 = 479$ kHz^2; total measurement time 11.0 h. Data were processed in nmrPipe [54] as follows: Lorentzian (−50 Hz) to Gaussian (+150) apodization, zero filling to 8192 complex points, Fourier transformation (t_3 to F3), and polynomial correction; apodization (−50, +200 Hz), zero filling to 256 complex points, t_2-to-F2 transformation; apodization (−15, +75 Hz), zero filling to 256 complex points, t_1-to-F1 transformation.

hands, even highly thermostable proteins such as ubiquitin [9,16] and GB1 [47], prepared with ~10–20 mM salt, remain viable for a period of only a few days to two weeks of experiments at 750 MHz, in comparison to several months at 500 MHz with similar decoupling amplitudes and MAS rates. We conclude that the sample deterioration is due primarily to RF-induced heating, and not the effects of centrifugal forces or macroscopic dehydration (which can be logically excluded by gravimetric analysis of samples before and after extended periods of spinning). At higher B_0 fields (e.g., 900 MHz ^{1}H frequency) such issues will be more critical, since the heating is proportional to the cube of the frequency.

The 1D ^{13}C and ^{15}N sensitivity with the scroll coil probe are compromised somewhat relative to the solenoid probe, due to the reduced Q of the scroll resonator at low frequency. However, with appropriate power handling considerations in the circuit design, sufficiently short ^{13}C and ^{15}N pulse widths can be achieved in the scroll coil probe, to perform 2D and 3D experiments where the benefits of high B_1 homogeneity and ^{1}H decoupling fields translate into improved polarization transfer efficiency and spectral resolution. We have presented one example of how these gains may be achieved for heteronuclear (^{15}N–^{13}C) 2D and 3D experiments. We anticipate that additional benefits will be derived from the excellent homogeneity of B_1 amplitude and phase over the sample, to enhance performance of existing multiple pulse sequences and potentially enable even more sophisticated schemes to be implemented in pro-

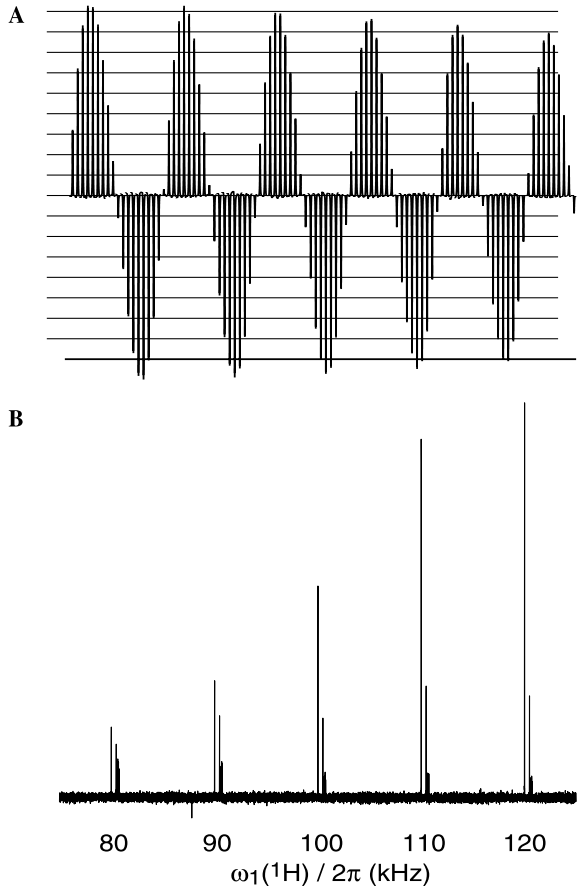

Fig. 5. (A) ^{1}H RF nutation profile at 750 MHz with the full available sample volume (3.2 mm rotor) packed with adamantane. The ^{1}H pulse width is incremented in 0.5 μs steps from 0 to 50 μs. The intensity of the signal after four complete (360°) nutations is greater than 90% of the maximum signal intensity (i.e., $I_{1530}/I_{90} > 90\%$). (B) Double cross polarization spectra of [U-^{13}C,^{15}N]*N*-acetyl-valine. The SPECIFIC CP condition from ^{15}N to the ^{13}Cα signal is utilized, with a contact time of 10 ms at $\omega(^{15}\mathrm{N})/2\pi = \sim 18$ kHz, $\omega(^{13}\mathrm{C})/2\pi = \sim 31$ kHz (at ~55 ppm) [21] with a ±500 Hz tangent ramp. The ^{1}H decoupling during the ^{15}N–^{13}C CP period was varied, resulting in nearly 50% overall ^{1}H–^{15}N–^{13}C efficiency at the highest decoupling, in comparison to the direct ^{1}H–^{13}C CP spectrum.

teins. Furthermore, the high-frequency scroll coil performance is well suited for ^{1}H detection, where sensitivity gains have already been demonstrated, even with probes optimized for low frequency observation [48–50]. The combination of high B_1 homogeneity, improved ^{1}H efficiency (sensitivity) and tolerance for high dielectric samples will be especially beneficial for application of these experiments to large proteins.

Acknowledgments

This research was supported by the University of Illinois (startup funds to C.M.R.), the Research Corporation (Research Innovation Award) and the National Science Foundation (CAREER Award, MCB 0347824). The authors thank Dr. Paul Molitor (VOICE NMR Facility, School of Chemical Sciences, University of Illinois) for technical assistance, and Dr. Knut Mehr (Varian, Inc., Palo Alto, California) for recommending the scroll coil as a resonator structure for SSNMR probes.

References

[1] S. Luca, H. Heise, M. Baldus, High-resolution solid-state NMR applied to polypeptides and membrane proteins, Accounts Chem. Res. 36 (2003) 858–865.
[2] S.J. Opella, F.M. Marassi, Structure determination of membrane proteins by NMR spectroscopy, Chem. Rev. 104 (2004) 3587–3606.
[3] M. Hong, Determination of multiple phi-torsion angles in proteins by selective and extensive ^{13}C labeling and two-dimensional solid-state NMR, J. Magn. Reson. 139 (1999) 389–401.
[4] R. Tycko, Y. Ishii, Constraints on supramolecular structure in amyloid fibrils from two-dimensional solid-state NMR spectroscopy with uniform isotopic labeling, J. Am. Chem. Soc. 125 (2003) 6606–6607.
[5] H.B.R. Cole, S.W. Sparks, D.A. Torchia, Comparison of the solution and crystal-structures of staphylococcal nuclease with ^{13}C and ^{15}N chemical-shifts used as structural fingerprints, Proc. Natl. Acad. Sci. USA 85 (1988) 6362–6365.
[6] J. Pauli, B. van Rossum, H. Forster, H.J.M. de Groot, H. Oschkinat, Sample optimization and identification of signal patterns of amino acid side chains in 2D RFDR spectra of the alpha-spectrin SH3 domain, J. Magn. Reson. 143 (2000) 411–416.
[7] A. Bockmann, A. Lange, A. Galinier, S. Luca, N. Giraud, M. Juy, H. Heise, R. Montserret, F. Penin, M. Baldus, Solid state NMR sequential resonance assignments and conformational analysis of the 2 × 10.4 kDa dimeric form of the *Bacillus subtilis* protein Crh, J. Biomol. NMR 27 (2003) 323–339.
[8] R.W. Martin, K.W. Zilm, Preparation of protein nanocrystals and their characterization by solid state NMR, J. Magn. Reson. 165 (2003) 162–174.
[9] T.I. Igumenova, A.J. Wand, A.E. McDermott, Assignment of the backbone resonances for microcrystalline ubiquitin, J. Am. Chem. Soc. 126 (2004) 5323–5331.
[10] F. Moll, T.A. Cross, Optimizing and characterizing alignment of oriented lipid bilayers containing gramicidin D, Biophys. J. 57 (1990) 351–362.
[11] A.E. Kelly, H.D. Ou, R. Withers, V. Dotsch, Low-conductivity buffers for high-sensitivity NMR measurements, J. Am. Chem. Soc. 124 (2002) 12013–12019.
[12] D.G. Gadian, F.N.H. Robinson, Radiofrequency losses in NMR experiments on electrically conducting samples, J. Magn. Reson. 34 (1979) 449–455.
[13] A. Detken, E.H. Hardy, M. Ernst, B.H. Meier, Simple and efficient decoupling in magic-angle spinning solid-state NMR: the XiX scheme, Chem. Phys. Lett. 356 (2002) 298–304.
[14] J. Pauli, M. Baldus, B. van Rossum, H. de Groot, H. Oschkinat, Backbone and side-chain ^{13}C and ^{15}N resonance assignments of the alpha-spectrin SH3 domain by magic angle spinning solid state NMR at 17.6 T, ChemBioChem 2 (2001) 101–110.
[15] F. Castellani, B. van Rossum, A. Diehl, M. Schubert, K. Rehbein, H. Oschkinat, Structure of a protein determined by solid-state magic-angle-spinning NMR spectroscopy, Nature 420 (2002) 98–102.
[16] T.I. Igumenova, A.E. McDermott, K.W. Zilm, R.W. Martin, E.K. Paulson, A.J. Wand, Assignments of carbon NMR

resonances for microcrystalline ubiquitin, J. Am. Chem. Soc. 126 (2004) 6720–6727.
[17] A. McDermott, T. Polenova, A. Bockmann, K.W. Zilm, E.K. Paulsen, R.W. Martin, G.T. Montelione, Partial NMR assignments for uniformly (C-13, N-15)-enriched BPTI in the solid state, J. Biomol. NMR 16 (2000) 209–219.
[18] A. Kubo, C.A. McDowell, Spectral spin diffusion in polycrystalline solids under magic-angle spinning, J. Chem. Soc. Faraday Trans. 1 (84) (1988) 3713–3730.
[19] K. Takegoshi, S. Nakamura, T. Terao, C-13-H-1 dipolar-assisted rotational resonance in magic-angle spinning NMR, Chem. Phys. Lett. 344 (2001) 631–637.
[20] A.E. Bennett, J.H. Ok, R.G. Griffin, S. Vega, Chemical shift correlation spectroscopy in rotating solids: radio-frequency dipolar recoupling and longitudinal exchange, J. Chem. Phys. 96 (1992) 8624–8627.
[21] M. Baldus, A.T. Petkova, J.H. Herzfeld, R.G. Griffin, Cross polarization in the tilted frame: assignment and spectral simplification in heteronuclear spin systems, Mol. Phys. 95 (1998) 1197–1207.
[22] D.M. Gregory, D.J. Mitchell, J.A. Stringer, S. Kiihne, J.C. Shiels, J. Callahan, M.A. Mehta, G.P. Drobny, Windowless dipolar recoupling—the detection of weak dipolar couplings between spin-1/2 nucleic with large chemical-shift anisotropies, Chem. Phys. Lett. 246 (1995) 654.
[23] Y.K. Lee, N.D. Kurur, M. Helmle, O.G. Johannessen, N.C. Nielsen, M.H. Levitt, Efficient dipolar recoupling in the NMR of rotating solids. A sevenfold symmetric radiofrequency pulse sequence, Chem. Phys. Lett. 242 (1995) 304–309.
[24] M. Hohwy, C.M. Rienstra, C.P. Jaroniec, R.G. Griffin, Fivefold symmetric homonuclear dipolar recoupling in rotating solids: application to double quantum spectroscopy, J. Chem. Phys. 110 (1999) 7983–7992.
[25] A. Brinkmann, M. Eden, M.H. Levitt, Synchronous helical pulse sequences in magic-angle spinning nuclear magnetic resonance: double quantum recoupling of multiple-spin systems, J. Chem. Phys. 112 (2000) 8539–8554.
[26] M. Carravetta, M. Eden, X. Zhao, A. Brinkmann, M.H. Levitt, Symmetry principles for the design of radiofrequency pulse sequences in the nuclear magnetic resonance of rotating solids, Chem. Phys. Lett. 321 (2000) 205–215.
[27] C.M. Rienstra, M. Hohwy, M. Hong, R.G. Griffin, 2D and 3D ^{15}N–^{13}C–^{13}C NMR chemical shift correlation spectroscopy of solids: assignment of MAS spectra of peptides, J. Am. Chem. Soc. 122 (2000) 10979–10990.
[28] C.E. Hughes, S. Luca, M. Baldus, Radio-frequency driven polarization transfer without heteronuclear decoupling in rotating solids, Chem. Phys. Lett. 385 (2004) 435–440.
[29] M. Ernst, Heteronuclear spin decoupling in solid-state NMR under magic-angle sample spinning, J. Magn. Reson. 162 (2003) 1–34.
[30] M. Ernst, A. Samoson, B.H. Meier, Low-power XiX decoupling in MAS NMR experiments, J. Magn. Reson. 163 (2003) 332–339.
[31] A. Addlagatta, S. Krzywda, H. Czapinska, J. Otlewski, M. Jaskolski, Ultrahigh-resolution structure of a BPTI mutant, Acta Crystallogr. Sect. D Biol. Crystallogr. 57 (2001) 649–663.
[32] S.O. Smith, S. Farr-Jones, R.G. Griffin, W.W. Bachovchin, Crystal versus solution structures of enzymes: NMR spectroscopy of a crystalline serine protease, Science 244 (1989) 961–964.
[33] S. Rozovsky, A.E. McDermott, The time scale of the catalytic loop motion in triosephosphate isomerase, J. Mol. Biol. 310 (2001) 259–270.
[34] V.R. Cross, R.K. Hester, J.S. Waugh, Single coil probe with transmission-line tuning for nuclear magnetic double resonance, Rev. Sci. Instrum. 47 (1976) 1486.
[35] F.D. Doty, R.R. Inners, P.D. Ellis, A multinuclear double-tuned probe for applications with solids or liquids utilizing lumped tuning elements, J. Magn. Reson. 43 (1981) 399–416.
[36] W. Froncisz, J.S. Hyde, The loop-gap resonator: a new microwave lumped element circuit ESR sample structure, J. Magn. Reson. 47 (1982) 515–521.
[37] M. Mehdizadeh, T.K. Ishii, J.S. Hyde, W. Froncisz, Loop-gap resonator: a lumped mode microwave resonant structure, IEEE Trans. Micro. 31 (1983) 1059–1063.
[38] M. Alecci, I. Nicholson, D.J. Lurie, A novel multiple-tuned radiofrequency loop-gap resonator for use in PEDRI, J. Magn. Reson. B 110 (1996) 82–86.
[39] F.H. Larsen, P. Daugaard, H.J. Jakobsen, N.C. Nielsen, Improving rf field homogeneity in solid-state MAS NMR using a loop-gap resonator, J. Magn. Reson. A 115 (1995) 283–286.
[40] D.G. Cory, J.T. Lewandowski, W. Maas, NMR probe for cross-polarization measurements, Bruker Instruments, Inc. United States Patent #5,539,315, July 23, 1996.
[41] S.C. Grant, L.A. Murphy, R.L. Magin, G. Friedman, Analysis of multilayer radio frequency microcoils for nuclear magnetic resonance spectroscopy, IEEE Trans. Magn. 37 (2001) 2989–2998.
[42] C. Mullen, J. Stringer, K. Mehr, Multiple tuned scroll coil, Varian, Inc., United States Patent (Pending).
[43] R.W. Martin, E.K. Paulson, K.W. Zilm, Design of a triple resonance magic angle sample spinning probe for high field solid state nuclear magnetic resonance, Rev. Sci. Instrum. 74 (2003) 3045–3061.
[44] M.C.K. Wiltshire, J.B. Pendry, I.R. Young, D.J. Larkman, D.J. Gilderdale, J.V. Hajnal, Microstructured magnetic materials for RF flux guides in magnetic resonance imaging, Science 291 (2001) 849–851.
[45] D.I. Hoult, R.E. Richards, The signal-to-noise ratio of the nuclear magnetic resonance experiment, J. Magn. Reson. 24 (1976) 71–85.
[46] C.S. Zuo, K.R. Metz, Y. Sun, A.D. Sherry, NMR temperature measurements using a paramagnetic lanthanide complex, J. Magn. Reson. 133 (1998) 53–60.
[47] W.T. Franks, D.H. Zhou, B.G. Money, D.T. Graesser, G. Sahota, C.M. Rienstra, Magic-angle spinning solid-state NMR spectroscopy of the B1 immunoglobin binding domain of protein G (GB1): ^{15}N and ^{13}C chemical shift assignments and conformational analysis, J. Am. Chem. Soc. (2004), submitted.
[48] B. Reif, C.P. Jaroniec, C.M. Rienstra, M. Hohwy, R.G. Griffin, ^{1}H–^{1}H MAS correlation spectroscopy and distance measurements in a deuterated peptide, J. Magn. Reson. 151 (2001) 320–327.
[49] I. Schnell, H.W. Spiess, High-resolution ^{1}H NMR spectroscopy in the solid state: very fast sample rotation and multiple-quantum coherences, J. Magn. Reson. 151 (2001) 153–227.
[50] E.K. Paulson, C.R. Morcombe, V. Gaponenko, B. Dancheck, R.A. Byrd, K.W. Zilm, Sensitive high resolution inverse detection NMR spectroscopy of proteins in the solid state, J. Am. Chem. Soc. 125 (2003) 15831–15836.
[51] S. Hediger, B.H. Meier, N.D. Kurur, G. Bodenhausen, R.R. Ernst, NMR cross-polarization by adiabatic passage through the Hartmann–Hahn condition (APHH), Chem. Phys. Lett. 223 (1994) 283–288.
[52] D. Marion, K. Wuthrich, Application of phase sensitive two-dimensional correlated spectroscopy (cosy) for measurements of ^{1}H–^{1}H spin–spin coupling-constants in proteins, Biochem. Biophys. Res. Commun. 113 (1983) 967–974.
[53] A.E. Bennett, C.M. Rienstra, M. Auger, K.V. Lakshmi, R.G. Griffin, Heteronuclear decoupling in rotating solids, J. Chem. Phys. 103 (1995) 6951–6958.
[54] F. Delaglio, S. Grzesiek, G.W. Vuister, G. Zhu, J. Pfeifer, A. Bax, Nmrpipe—a multidimensional spectral processing system based on unix pipes, J. Biomol. NMR 6 (1995) 277–293.